scientific reports

OPEN

Structural basis of divergent substrate recognition and inhibition of human neurolysin

Ke Shi[1], Sounak Bagchi[2], Jordis Bickel[2], Shiva H. Esfahani[2,3], Lulu Yin[1], Tiffany Cheng[1], Vardan T. Karamyan[2,3✉] & Hideki Aihara[1✉]

A zinc metallopeptidase neurolysin (Nln) processes diverse bioactive peptides to regulate signaling in the mammalian nervous system. To understand how Nln interacts with various peptides with dissimilar sequences, we determined crystal structures of Nln in complex with diverse peptides including dynorphins, angiotensin, neurotensin, and bradykinin. The structures show that Nln binds these peptides in a large dumbbell-shaped interior cavity constricted at the active site, making minimal structural changes to accommodate different peptide sequences. The structures also show that Nln readily binds similar peptides with distinct registers, which can determine whether the peptide serves as a substrate or a competitive inhibitor. We analyzed the activities and binding of Nln toward various forms of dynorphin A peptides, which highlights the promiscuous nature of peptide binding and shows how dynorphin A (1–13) potently inhibits the Nln activity while dynorphin A (1–8) is efficiently cleaved. Our work provides insights into the broad substrate specificity of Nln and may aid in the future design of small molecule modulators for Nln.

The availability and actions of bioactive peptides are modulated by a group of enzymes known as peptidases. Many of these enzymes are metallopeptidases which catalyze the peptide bond hydrolysis with the help of a zinc ion cofactor. Neurolysin (Nln) is one of these peptidases and belongs to the M3 family of metallopeptidases that also includes thimet oligopeptidase (TOP) and several other members[1]. Nln is widely expressed in mammalian tissues, with the highest expression in the brain and liver, and depending on the cell type it is found in the cytosol, mitochondria, plasma membrane and extracellularly[2]. Biochemical and pharmacological properties of Nln have been studied in detail since its discovery[3,4], whereas in recent years more studies have focused on delineating its (patho)physiological function[5–8]. While most studies have focused on the extracellular peptide substrates of Nln, there is evidence that mitochondrial and cytosolic peptides are also processed by this peptidase[8,9].

Structural studies focusing on understanding the substrate recognition, catalysis and modulation of Nln activity continue to be important for the development of pharmacological and chemical biological tools to study this enzyme. Nln and related peptidases share an overall prolate ellipsoid shape comprising two long, primarily α-helical domains[10]. The two domains are divided by a deep and narrow channel, which accommodates substrate peptides. The active site of Nln is located near the bottom of the channel and about midway along its long axis length, and it features a pair of α-helices harboring His474, His478, and Glu503 that coordinate the essential Zn ion and Glu475 that serves to activate the nucleophilic water molecule. A comparison between multiple Nln crystal structures shows that the channel closes around the bound peptide via a hinge-like motion of the two domains toward each other, which can be blocked by the binding of an allosteric inhibitor away from the active site[8,11,12]. Small molecule activators of Nln are also being pursued[13,14], because the Nln activity is proposed to be neuro/cerebroprotective in brain after stroke by virtue of inactivating neuro/cerebrotoxic peptides and generating neuro/cerebroprotective ones[15,16].

Among the diverse set of neuropeptides cleaved by Nln are angiotensins, neurotensin, bradykinin, luteinizing hormone-releasing hormone, substance P, and dynorphin A (Dyn A)[17]. Dynorphins are a family of opioid peptides that are formed through the processing of a precursor prodynorphin by proprotein convertase 2[18], and they serve as an agonist for kappa opioid receptors (KORs) in the central and peripheral nervous systems to

[1]Department of Biochemistry, Molecular Biology and Biophysics, University of Minnesota, Minneapolis, MN 55455, USA. [2]Department of Pharmaceutical Sciences, Texas Tech University Health Sciences Center, Amarillo, TX 79106, USA. [3]Department of Foundational Medical Studies, Oakland University, Rochester, MI 48309, USA. ✉email: vkaramyan@oakland.edu; aihar001@umn.edu

regulate pain perception and memory. The longer and shorter forms, Dyn A (1–17) and Dyn A (1–8), respectively, have been reported to be cleaved by Nln between Leu5 and Arg6, whereas Dyn A (1–17) is additionally cleaved at a unique site between Lys11 and Leu12[17,19]. Curiously, however, a form of dynorphin with an intermediate length, Dyn A (1–13), has been reported to serve as a potent competitive inhibitor of Nln and is not cleaved[9,13,17]. The molecular mechanism underlying the distinct cleavability among the similar dynorphin peptides by Nln is unknown. Because the high-resolution structure of a Nln-peptide complex is only available for neurotensin[8], a general understanding of how Nln interacts with diverse bioactive peptides is lacking. In this study, we sought to characterize Nln interaction with various substrates, including different forms of dynorphins, to gain insights into the substrate selectivity of Nln.

Results

Nln activities on diverse dynorphin A peptides

Previous studies have investigated the processing of different dynorphin peptides by Nln, but a comprehensive analysis comparing Nln-mediated cleavage of various forms of dynorphin is lacking. Thus, we examined in parallel the cleavage by Nln of Dyn A (1–7), Dyn A (1–8), Dyn A (1–9), Dyn A (1–10), Dyn A (1–11), Dyn A (1–12), Dyn A (1–13), and Dyn A (1–17). The different forms of Dyn A peptides were incubated with Nln and the amount of uncleaved peptides was analyzed by mass spectrometry. The liquid chromatography–mass spectrometry (LC–MS) results suggest that Dyn A (1–8) is degraded best among the studied Dyn A peptides; 68.5% (95% CI 58.9–78.1%) uncleaved peptide quantified (Fig. 1). In addition, Dyn A (1–9) and Dyn A (1–17) were also degraded, although to a lesser and comparable extent; 79.2% (95% CI 72.1–86.3%) and 87.5% (95% CI 83.3–91.1%) uncleaved peptide quantified, respectively. The other Dyn A peptides were not significantly degraded by Nln.

To gain information about the binding affinity of these Dyn A peptides to Nln, we also carried out competition experiments with different concentrations of the peptides against a quenched fluorogenic substrate of Nln, Mca–Pro–Leu–Gly–Pro–D–Lys(DNP)–OH, which binds to the active site of the peptidase and is hydrolyzed. Consistent with our expectations, Dyn A (1–13) showed the highest affinity for Nln, with $K_i = 1.0$ μM (95% CI 0.9–1.1 μM). Dyn A (1–12) had a comparably high affinity, $K_i = 0.9$ μM (95% CI 0.8–1.1 μM), followed by Dyn A (1–9) and Dyn A (1–17), which showed K_i values of ~6 μM. The rest of the Dyn A peptides showed lower affinity to Nln (Fig. 2), with no good correlation between the binding affinities and the documented degree of hydrolysis (Fig. 1).

Nln binding to diverse dynorphin A peptides

Next, we used N-terminally fluorescently labeled peptides, which have the same amino acid sequences as Dyn A but with 5-carboxyfluorescein (FAM) replacing Tyr1, to investigate the binding of Dyn A peptides to Nln. A plot of fluorescence polarization (FP) changes as a function of Nln concentration showed that Nln binds to FAM-^{2}GGFLRRIRPKLK^{13} with an equilibrium dissociation constant (K_D) of 1.47 μM (95% CI 1.44–1.50 μM) (Fig. 3a). This matches closely the Ki value of Dyn A (1–13) in inhibiting Nln in the enzymatic assay presented in Fig. 2 (1.0 μM) and our published value of 1.19 μM[13], validating that FAM-^{2}GGFLRRIRPKLK^{13} mimics the competitive binding of Dyn A (1–13) in the substrate-binding site. We further measured the affinity of a panel of Dyn A mimics, FAM-^{2}GGFLRRI^8, FAM-^{2}GGFLRRIRP^{10}, FAM-^{2}GGFLRRIRPKLK^{13}, and FAM-^{2}GGFLRRIRPKLKWDNQ^{17} to Nln E475A, a catalytically inactive mutant of Nln incapable of cleaving and turning over these peptides. FP data showed that these peptides, which mimic Dyn A (1–8), Dyn A (1–10), Dyn A (1–13), and Dyn A (1–17), respectively, bind to Nln with progressively higher affinities with K_D values of 23.7 (95% CI 20.7–27.4) μM, 8.46
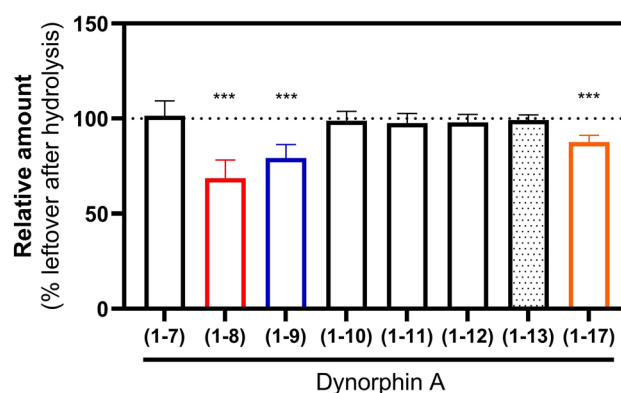

Figure 1. Hydrolysis of dynorphin A peptides by Nln. Each of the Dyn A peptides (20 μM) was incubated with recombinant human Nln (2 nM) or buffer (as control) for 45 min followed by measurement of the peptide level by mass-spectrometry analysis (n = 4 independent experiments, repeated twice; ***P < 0.001 in comparison with control condition without Nln). The dotted black line indicates the relative amount of peptides in control samples which did not contain Nln; mean ± SD are presented.
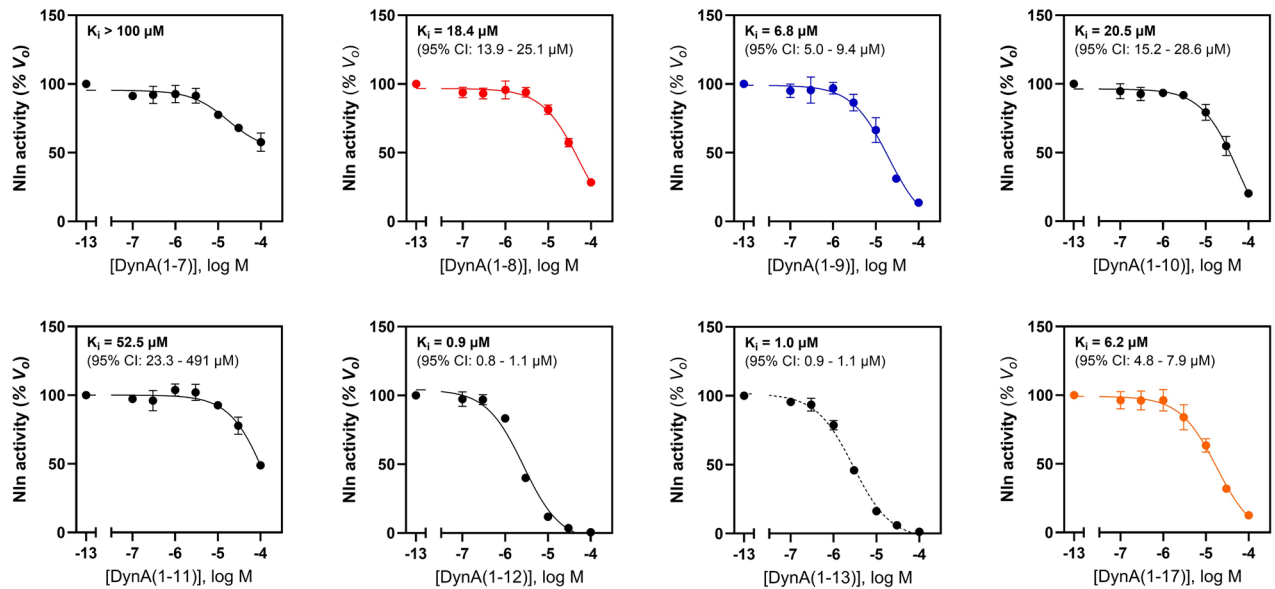
Figure 2. The affinity dynorphin A peptides for Nln determined from competition experiments with the synthetic substrate. Concentration-dependent effect of Dyn A peptides on the hydrolysis of the quenched fluorescence substrate by recombinant human Nln by is shown (n = 4 independent experiments with duplicate samples for each concentration; mean ± SD are presented). Note that the initial velocity of hydrolysis in the absence of a Dyn A peptide corresponds to 100% on the vertical axis (basal activity) and −13 on the horizontal axis.
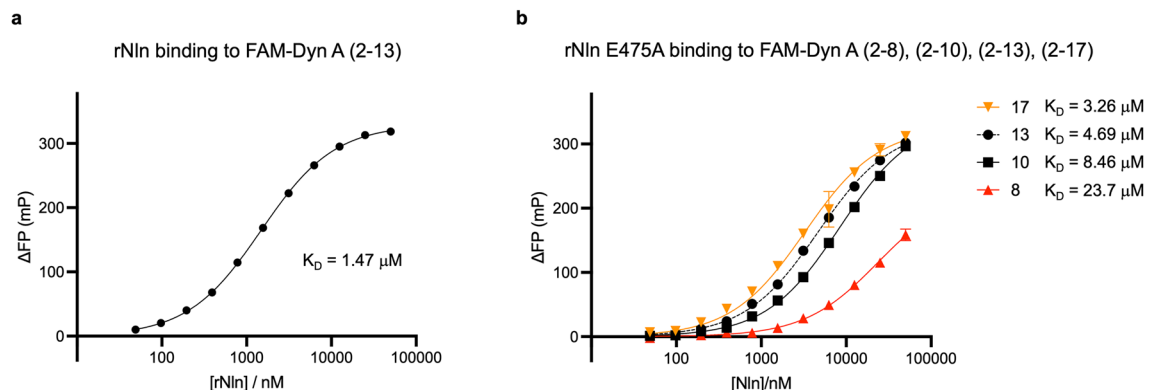

Figure 3. Nln binding to dynorphin A peptides with different lengths. (**a**) Binding of an N-terminally fluorescein-labeled Dyn A (2–13) peptide to catalytically active Nln, as probed by fluorescence polarization. Changes in fluorescence polarization (mP) from the control sample containing no Nln were plotted against the total Nln concentration in the reaction. (**b**) Binding of fluorescein-labeled Dyn A mimic peptides with various lengths to an inactive Nln mutant (E475A). The K_D values were determined by fitting the data to the one site, specific binding with ligand depletion model. Error bars show standard deviation among two (**a**) or three (**b**) technical replicates.

(7.95–9.00) µM, 4.69 (4.42–4.98) µM, and 3.26 (2.88–3.68) µM, respectively, suggesting that additional contacts made by the extended peptides contribute to affinity (Fig. 3b).

hNln-peptide complex structures

The experiments described above establish that Nln cleaves Dyn A (1–8), (1–9), and (1–17), but is inhibited by Dyn A (1–12) and (1–13). On the other hand, all Dyn A variants tested in the FP experiment showed binding to Nln, with progressively higher affinity for longer variants. These results suggest that the different forms of Dyn A peptides may interact with Nln in distinct fashions. To understand the structural basis of the differential interaction, we crystallized human Nln (hNln) in complex with either Dyn A (1–8) or Dyn A (1–13) under similar crystallization conditions. In addition, we co-crystallized hNln with other known substrate peptides, namely, neurotensin, angiotensin I, and bradykinin. The crystal structures were determined by molecular replacement phasing and refined to a resolution ranging from 1.95 to 2.88 Å (Table 1). Although all hNln-peptide crystals

	Dynorphin A (1–13)	Dynorphin A (1–8)	Angiotensin I	Bradykinin	Neurotensin
Data collection					
Resolution range (Å)	79.9–1.99 (2.06–1.99)[1]	57.3–2.12 (2.20–2.12)[2]	51.4–2.49 (2.58–2.49)[3]	96.6–2.88 (2.99–2.88)[4]	48.5–1.95 (48.5–1.95)
Space group	$P2_12_12$	$P2_12_12$	$P2_1$	$P2_12_12$	$P2_12_12_1$
Unit cell					
a, b, c (Å)	142.07, 60.26, 95.55	143.17, 60.12, 95.73	101.08, 60.58, 147.75	143.83, 60.51, 96.56	59.49, 150.36, 188.19
α, β, γ (°)	90, 90, 90	90, 90, 90	90, 106.57, 90	90, 90, 90	90, 90, 90
Total reflections	145,128 (7684)	399,584 (19,296)	117,633 (7290)	110,669 (5746)	783,426 (21,292)
Unique reflections	48,703 (734)	42,141 (627)	33,504 (63)	15,148 (135)	123,468 (4926)
Multiplicity	3.0 (3.2)	9.5 (9.2)	3.5 (4.4)	7.3 (7.6)	6.3 (4.3)
Compl. (%, SPH)	84.9 (25.8)	88.7 (29.2)	55.3 (8.5)	77.0 (18.1)	99.0 (80.8)
Compl. (%,ELLIP)	93.0 (51.7)	94.3 (47.5)	89.2 (57.8)	92.6 (49.5)	n.a.
$<I/\sigma(I)>$	9.7 (1.4)	10.3 (1.4)	5.6 (1.5)	5.9 (1.3)	9.3 (0.5)
R_{merge}	0.055 (0.823)	0.138 (2.33)	0.171 (0.943)	0.278 (1.89)	0.160 (2.526)
R_{meas}	0.067 (0.981)	0.146 (2.46)	0.202 (1.08)	0.299 (2.03)	0.192 (3.15)
$R_{p.i.m}$	0.037 (0.528)	0.047 (0.798)	0.106 (0.512)	0.108 (0.718)	0.071 (1.471)
$CC_{1/2}$	0.998 (0.586)	0.995 (0.359)	0.991 (0.561)	0.992 (0.442)	0.995 (0.157)
Refinement					
Refl. for R_{work}	48,703 (734)	42,141 (627)	33,504 (63)	15,148 (135)	123,399 (11,108)
Refl. for R_{free}	2422 (29)	2076 (38)	1630 (3)	769 (12)	6091 (561)
R_{work}/R_{free}	0.195/0.218	0.213/0.249	0.238/0.286	0.219/0.256	0.201/0.234
Non-H atoms	5729	5525	10,838	5443	12,091
Macromolecules	5439	5433	10,828	5416	11,000
Ligands	37	14	2	1	90
Solvent	253	78	8	26	1001
Ave. B-factor (Å^2)	48.03	49.11	42.90	51.18	43.22
Macromolecules	47.81	49.11	42.90	51.24	42.76
Ligands	72.14	62.96	121.34	176.46	54.62
Solvent	49.25	47.08	29.82	32.84	47.21
rms deviation					
Bond lengths (Å)	0.002	0.001	0.001	0.001	0.002
Bond angles (°)	0.50	0.40	0.40	0.41	0.57
PDB ID	8VJU	8VJV	8VJW	8VJX	8VJY

Table 1. X-ray data collection and refinement statistics. Statistics for the highest-resolution shell are shown in parentheses. [1]Final resolution 2.15 Å along $a^\star$, 1.98 Å along $b^\star$, 2.02 Å along $c^\star$ [2]Final resolution 2.12 Å along $a^\star$, 2.20 Å along $b^\star$, 2.19 Å along $c^\star$ [3]Final resolution 3.50 Å along $0.670a^\star - 0.742c^\star$, 2.47 Å along $b^\star$, 2.90 Å along $0.381a^\star + 0.925c^\star$ [4]Final resolution 2.88 Å along $a^\star$, 2.94 Å along $b^\star$, 3.42 Å along $c^\star$

were obtained in essentially the same crystallization condition, they had differences in crystal packing, resulting in three crystal forms with different space groups. The crystallographic asymmetric unit (a.s.u.) contains single hNln molecule for the structure with Dyn A (1–8), Dyn A (1–13), or bradykinin, whereas there are two hNln molecules for the structure with angiotensin I or neurotensin.

The overall structure of hNln bound to the substrate or inhibitor peptides is similar to the 'closed' conformation previously reported for the structure of a catalytic mutant (E475Q) of hNln bound to neurotensin[8], with an overall root-mean-square-deviation (r.m.s.d.) ranging from 0.51 to 0.72 Å. The two domains of hNln close around the bound peptide in comparison to the 'open' conformations of Nln reported earlier[10,11], completely burying the peptide in the interior of the protein (Fig. 4a, b). A cut-away view of hNln bound to Dyn A (1–13) shows a large cavity in the interior of hNln in the closed conformation, which narrows near the Zn-bound active site to give an overall 'dumbbell-like' shape (Fig. 4c, d).

Distinct hNln-dynorphin interactions
Despite the overall high similarity, our hNln structures show remarkably diverse binding modes of the various peptides. The 2.12 Å resolution structure of hNln with Dyn A (1–8) ([1]YGGFLRRI[8]) shows strong electron density for [6]RR[7] downstream of the active site, consistent with the expected cleavage between Leu5 and Arg6 (Fig. 5a). The two arginine residues occupy the S2′/S3′ sites. This is reminiscent of the previously reported hNln structure with neurotensin (PDB ID: 5LUZ)[8], in which the cleaved product, [10]YIL[13], was bound with a "+1" register in the S2′/S3′/S4′ sites. A separate segment of electron density, albeit less well defined, best fits [1]YGGF[4] positioned such that Gly3 is at the S1 and Phe4 at the S1′ positions, suggesting that the upstream (N-terminal) residues also shifted toward the C-terminus after cleavage and occupied the active site.
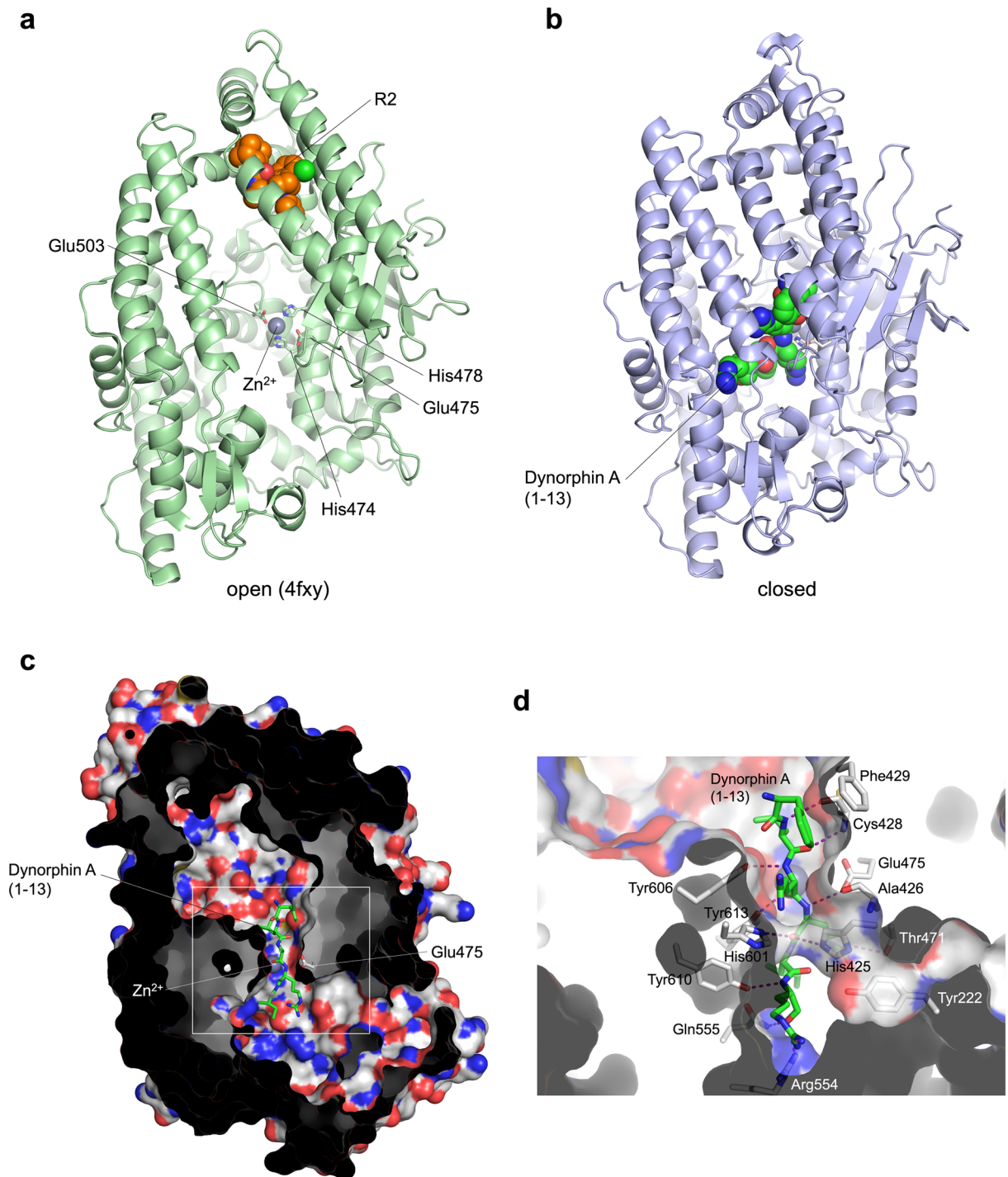
Figure 4. Nln in the closed conformation features a dumbbell-shaped interior cavity. (**a**) Crystal structure of rat Nln in the open conformation, in complex with an allosteric inhibitor R2[11]. (**b**) Our crystal structure of hNln in the closed conformation, in complex with Dyn A (1–13). The gray sphere represents the zinc ion in the active site. Active site residues are show in sticks. (**c**) A cut-away view of hNln bound to Dyn A (1–13). The protein surface facing the solvent is colored according to the atom type: white for carbon, blue for nitrogen, and red for oxygen. The other (non solvent-accessible) side of the protein surface is colored in black. (**d**) Zoomed view of the boxed area in the left panel, with a transparent protein surface. Dyn A (1–13) is in green sticks. Surrounding hNln side chains are shown, with hydrogen bonds indicated by purple dashed lines.

In contrast to the structure with a cleaved substrate peptide above, the structure with Dyn A (1–13) ([1]YGGFL-RRIRPKLK[13]) shows continuous electron density corresponding to [4]FLRRIR[9] centered on the active site, which
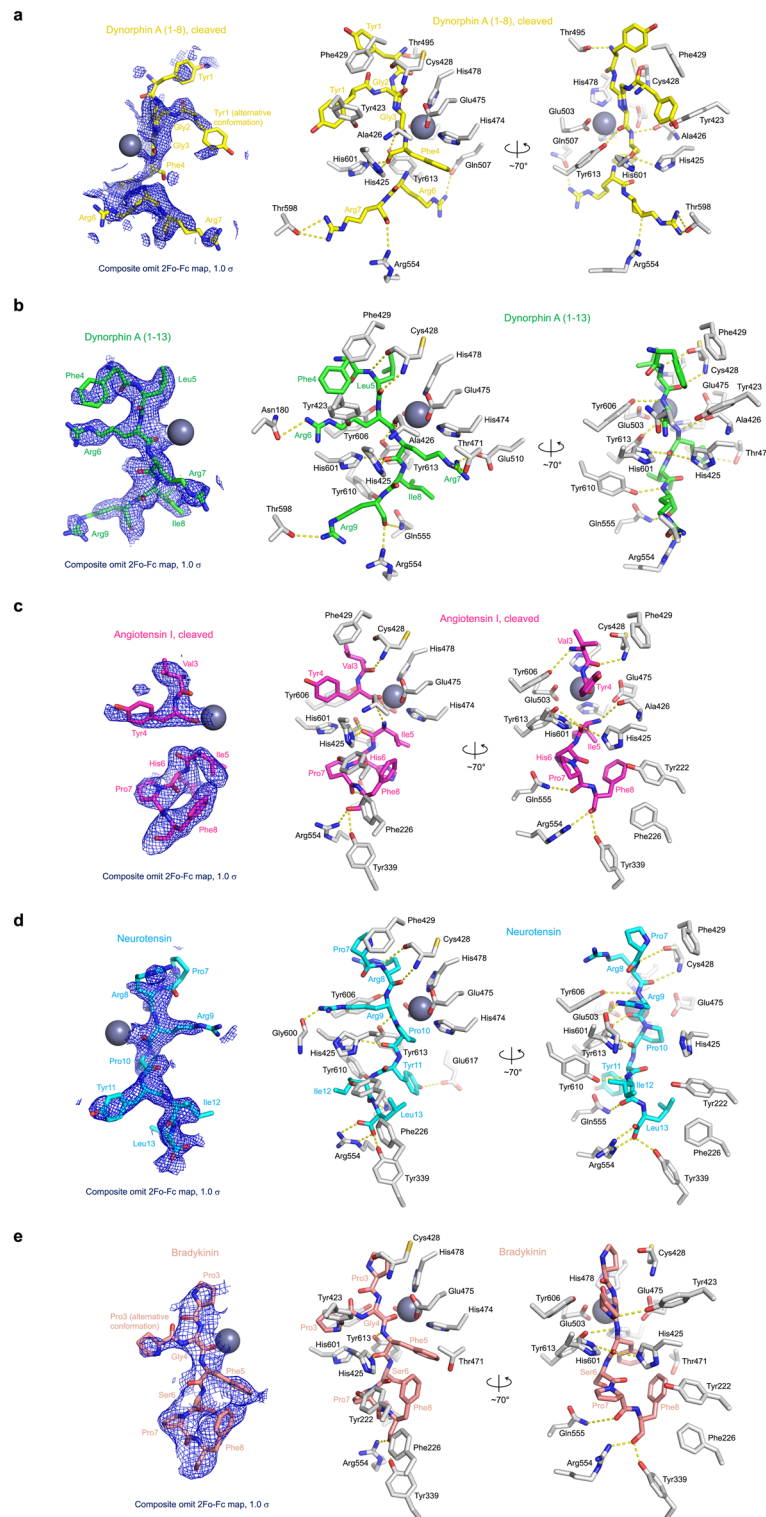
Figure 5. Nln crystal structures with various peptides. (**a**) Cleaved Dyn A (1–8) bound to human Nln. Left: Weighted 2Fo–Fc composite omit electron density map contoured at 1.0 σ above the mean level. Right: Interaction with the surrounding Nln residues. Hydrogen bonds and salt bridges are indicated by yellow dashed lines. The gray sphere represents the zinc ion in the Nln active site. The residues 5 (Leu) and 8 (Ile) were not modeled due to poor density. (**b**) Uncleaved Dyn A (1–13) bound to human Nln. The residues 1–3 and 10–13 were not modeled due to poor density. (**c**) Cleaved angiotensin I bound to human Nln. The residues 1–2 and 9–10 were not modeled due to poor density. (**d**) Uncleaved neurotensin bound to human Nln. The residues 1–6 were not modeled due to poor density. (**e**) Uncleaved bradykinin bound to human Nln. The residues 1–2 and 9 were not modeled due to poor density.

remained uncleaved (Fig. 5b). The observation that dynorphin A (1–13) binds to the active site of Nln but does not get cleaved is consistent with the previous reports and our data presented above indicating that it serves as a competitive inhibitor. The structure at 1.99 Å resolution suggests that the peptide is bound with Arg6 and Arg7 occupying the S1 and S1′ positions, respectively. Thus, Dyn A (1–13) is bound with a register offset by one residue (shifted toward the N-terminus, −1) compared to the binding mode expected for the cleavage between Leu5 and Arg6. The observation explains why Dyn A (1–13) is not readily cleaved by Nln, despite sharing the same N-terminal sequence with Dyn A (1–8).

hNln bound to cleaved angiotensin I

The 2.49 Å resolution crystal structure of hNln with angiotensin I ([1]DRVYIHPFHL[10]) shows discontinuous electron density corresponding to [3]VY[4] and [5]IHPF[8] in both molecules in the a.s.u., consistent with a cleavage between Tyr4 and Ile5 (Fig. 5c). The carboxyl group of Tyr4 at the P1 position interacts with the zinc ion in the active site. The residues outside those observed are presumably flexible. Although Nln has been shown to cleave angiotensin I between Pro7 and Phe8[20], angiotensin (1–4) is known to be generated when angiotensin II ([1]DRVYIHPF[8]) is cleaved by Nln[21,22], suggesting that angiotensin I could share the same binding mode for Nln with angiotensin II.

Neurotensin and bradykinin bound to hNln

Unexpectedly, binding in a shifted register to misalign the known cleavage sites with the active site, as observed for Dyn A (1–13), was also observed for two of the substrate peptides. In the structure of hNln with neurotensin ([1]pQLYENKPRRPYIL[13]; the canonical cleavage site is between Pro10 and Tyr11) at 1.95 Å resolution, both molecules in the a.s.u. showed Pro7–Leu13 of neurotensin bound with Arg9 and Pro10 occupying the S1 and S1′ positions, respectively, and the peptide remained uncleaved (Fig. 5d). Similarly, the structure of hNln with bradykinin ([1]RPPGFSPFR[9]; the canonical cleavage site is between Phe5 and Ser6) at 2.88 Å resolution showed Pro3–Phe8 of the uncleaved peptide bound with Gly4 and Phe5 occupying the S1 and S1′ positions, respectively (Fig. 5e). Thus, in both cases, the substrate peptide is bound with the expected scissile peptide bond positioned between the S1′ and S2′ positions, i.e., shifted toward the C-terminus (+1) compared to the binding mode for the expected cleavage site.

Conserved and unique features of hNln-peptide interaction

A comparison between our hNln-peptide complex structures highlights that the substrate-binding cavity of hNln can accommodate remarkably diverse peptides with dissimilar sequences without making large conformational changes (Fig. 6). The binding of these peptides is supported by an abundance of polar contacts: the residues positioned upstream of the active site (S2) form a β-sheet-like backbone interaction with hNln Cys428 from β6, whereas both the main chain and side chain atoms of the peptide downstream of the active site (S1′, S2′, S3′…) make hydrogen bonds or salt bridges with side chain atoms from hNln. The carbonyl group oxygen of the residue at S1′ position receives bifurcated hydrogen bonds donated by His425 and His601 in the structures with angiotensin I, Dyn A, and bradykinin, which produces the most constricted point of the peptide-binding cavity (Figs. 4d and 5a–e). The substrate interaction in this region also involves Tyr606 and Tyr613, which are hydrogen bonded to the backbone amide nitrogen and carbonyl oxygen atoms, respectively, of the P1 amino acid. Tyr606 was reported to play a key role in subsite S1[23], consistent with the structural observations. However, in both molecules in the a.s.u. of the neurotensin-bound structure, His425 side chain is flipped away from the peptide (Fig. 5d). An adjacent residue Tyr222 also shows a positional variation, shifting by ~ 1.5 Å towards a Phe side chain at the S4′ position in the angiotensin and bradykinin-bound structures (Fig. 5c, e). Thus, there is flexibility in this region lining the peptide-binding cavity of hNln, which may facilitate substrate-binding or catalysis. Hydrophobic side chains from the peptides also make favorable contacts with Nln residues Phe226 and Phe429.

Discussion

Nln processes a remarkably diverse set of peptide substrates with no significant sequence similarity, and our observations help to understand the basis of its broad substrate selectivity. The series of hNln-peptide complex structures reported here show that the peptide binding by Nln is highly flexible, which is highlighted by distinct modes of binding for Dyn A (1–8) and Dyn A (1–13). The central cavity of Nln also readily binds known Nln substrates in alternative registers, as observed for neurotensin and bradykinin, in which the canonical cleavage site is not aligned with the active site. These non-productive binding modes of substrate peptides could occur in solution and modulate the Nln activity. In addition, we observed that angiotensin I (1–10) could be cleaved between Tyr[4] and Ile[5] as reported for angiotensin II (1–8)[19], besides the previously reported site between Pro7 and Phe8[20]. This promiscuous peptide-binding and cleavage may reflect that the large dumbbell-shaped interior cavity of Nln can physically accommodate peptides with diverse sequences. In addition, many key contacts are made by Nln to the peptide backbone atoms, which could make the thermodynamics of binding relatively insensitive to the peptide sequence. In the absence of a strong sequence preference in binding, the preferred register of binding for a given peptide could be dictated by distal elements. In the case of Dyn A (1–8) vs. Dyn A (1–13), the differential binding is likely to be caused by additional contacts made by the C-terminal portion ([9]RPKLK[13]) including its steric effect, which may push Dyn A (1–13) to bind with "−1" register. Previous studies showed that Nln cleaves peptides sharing the same core sequence at different positions depending on the peptide length and sequence context[24,25], which is consistent with the flexible nature of binding. Furthermore, we did not observe a good correlation between the affinities of Dyn A peptides and the extent of their hydrolysis by Nln, which appears to be consistent with observations reported for other enzymes and their respective substrates[26].

Despite the non-selective nature of binding, peptide cleavage by Nln is more context-dependent, as exemplified by the structures of hNln in complex with uncleaved Dyn A (1–13). Dyn A (1–13) is not cleaved when
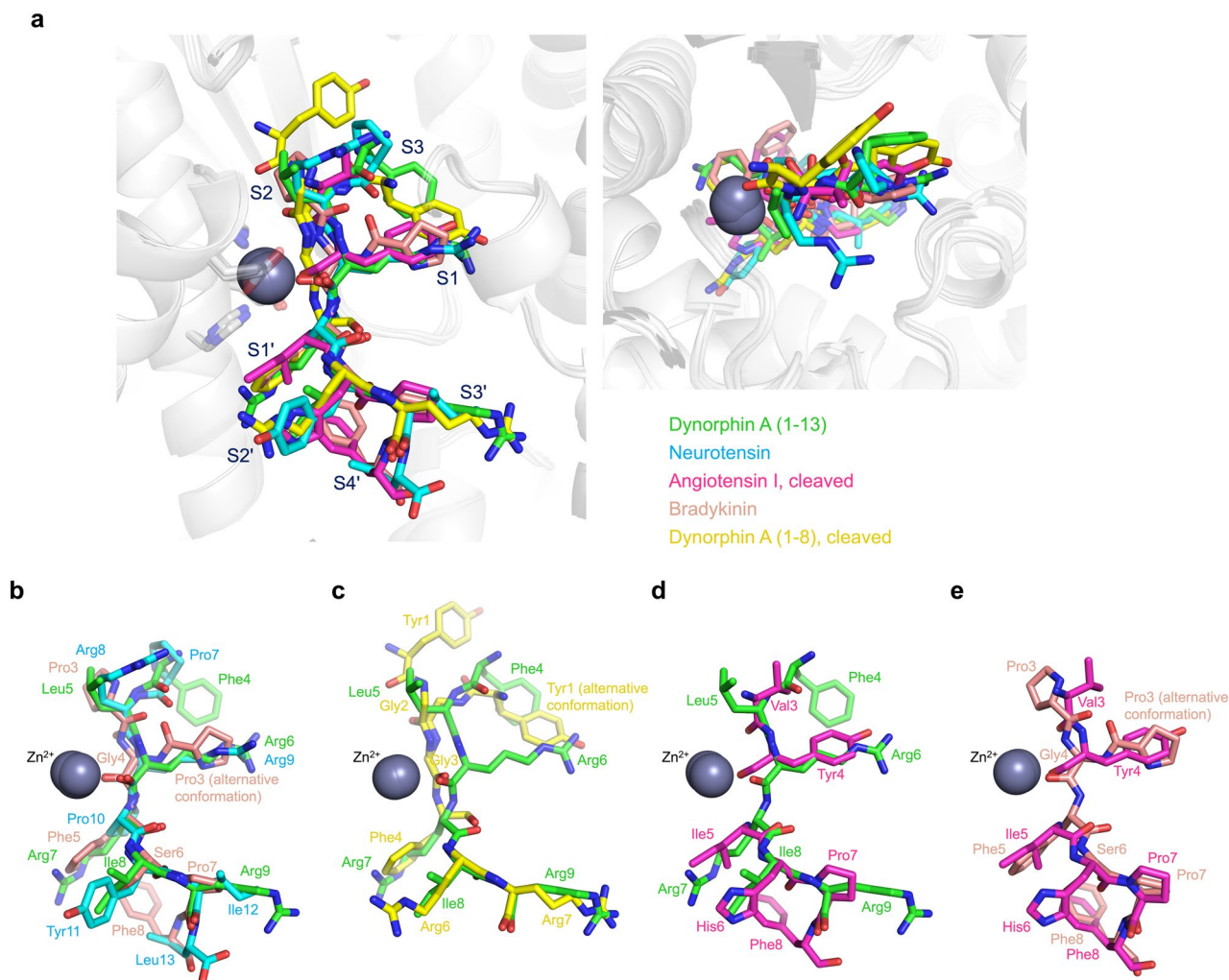
Figure 6. Superpositions of various peptides from the hNln-peptide structures determined in this study. (**a**) Two different views of a superposition of all five peptides. hNln is shown in a semitransparent ribbon schematic with its active site residues (His474, Glu475, His478, Glu503) as sticks. The gray sphere represents the zinc ion in the active site. Locations of the subsites on hNln that bind the substrate amino acid residues (S1–S3 and S1′–S4′ for the N-terminal and C-terminal side of the cleavage site, respectively) are indicated. The peptides are color-coded. (**b**) A superposition of the three uncleaved peptides: Dyn A (1–13), neurotensin, and bradykinin. (**c**) Dyn A (1–13) and cleaved Dyn A (1–8). (**d**) Dyn A (1–13) and cleaved angiotensin I. (**e**) Bradykinin and cleaved angiotensin I. Note the similarity for the residues 5–8 of both peptides.

Arg6 and Arg7 occupy the S1 and S1′ positions of Nln. Similarly, neurotensin positioned with Arg9 and Pro10 occupying the S1 and S1′ positions, respectively, remained uncleaved. Although P1 and P1′ amino acids flanking the scissile peptide bond in known Nln substrates are divergent without a clear consensus, arginine is not found at P1 in natural Nln substrates. It is possible that the conformation or positioning of the scissile peptide bond is not optimal for catalysis in these sequence contexts. Nln and TOP, a zinc metallopeptidase closely related to Nln, were shown to cleave neurotensin at distinct sites, and their specificities can be reversed by mutating Nln residues Arg470 and Thr499[27,28]. These two residues are positioned inside the substrate-binding pocket on either side of the active site. While not making specific polar contacts with the substrate peptide in our crystal structures, they are near the substrate peptide; for instance, Arg470 is within a distance for van der Waals contact from the Arg7 side chain of Dyn A (1–13) in our structure. Subtle changes in nearby residues are likely to modulate the conformation of the bound substrate and affect the catalysis. Further studies are needed to understand the potentially subtle but critical differences that distinguish pro-cleavage from non-catalytic complexes.

In conclusion, our work reveals at substantially improved resolutions the remarkable plasticity of Nln to interact with both cleaved and uncleaved peptides of diverse amino acid sequences. The structural information could be instrumental in the future development of small molecule modulators for Nln for therapeutic applications.

Methods

Protein purification

hNln (Ser38–Pro704) used in crystallography experiments was expressed from a codon-optimized synthetic gene with an N-terminal 6xHis-Sumo tag in *E. coli* strain BL21(DE3) and purified using nickel-affinity and

size-exclusion chromatography (SEC). The SEC elution profile and SDS–PAGE image are shown in Supplementary Fig. S1. The 6xHis-Sumo tag was removed by a Sumo protease (Ulp1) treatment before the SEC step. rNln (Met37–Ser704) with or without the E475A mutation used in fluorescence anisotropy experiments were expressed from a codon-optimized synthetic gene with a non-cleavable C-terminal 6xHis-tag in *E. coli* strain BL21(DE3) and purified as above. Purified proteins were concentrated by ultrafiltration in 20 mM Tris–HCl, pH 7.4, 0.5 M NaCl, 5 mM β-mercaptoethanol, frozen in liquid nitrogen, and stored at -80 °C. hNln (Ser38-Pro704) used in the activity assays (Figs. 1, 2) was expressed with an N-terminal 6xHis-tag using the pBAD/His C vector essentially as described in our previous publications[13,20]. The N-terminal 6xHis-tag was not removed from the final preparation. The purified protein dissolved in 50 mM Tris, pH 7.2, 100 mM NaCl, 0.05% Tween 20 (1.5–2 mg mL⁻¹) was frozen in liquid nitrogen in small volume aliquots, and stored at – 80 °C.

X-ray crystallography

hNln (38–704) at ~ 30 mg mL⁻¹ was mixed with various peptides (Phoenix Pharmaceuticals) at 1 mM final concentration and subjected to crystallization via hanging drop vapor diffusion. The drops were formed by mixing equal volumes of the hNln-peptide complex and the reservoir solution consisting of 17.5–30% polyethylene glycol 3350 and 50–125 mM Bis–Tris HCl buffer, pH 6.5. Crystals in thin plate morphology grew in 3–4 days after incubation at 20 °C (Supplementary Fig. S2). The crystals were cryo-protected by brief soaking in the reservoir solution supplemented with 20% ethylene glycol and flash-cooled in liquid nitrogen. X-ray diffraction data were collected at beamlines 24-ID-C and 24-ID-E of the advanced photon source (APS) and processed using XDS. The structures were determined by molecular replacement phasing with PHASER using the structure of hNln E475Q mutant (PDB ID: 5LUZ, chain A)[8] as the search model. Atomic models were built using COOT[29] and refined using PHENIX[30]. A summary of data collection and model refinement statistics is shown in Table 1. Structural figures (Figs. 4, 5, 6) were generated using PyMOL Ver. 3.0.3 (https://www.pymol.org/).

Fluorescence anisotropy

N-terminally FAM-labeled Dyn A (2–8), Dyn A (2–10), Dyn A (2–13), and Dyn A (2–17) were chemically synthesized and HPLC-purified to > 90% purity by BIOMATIK. The peptides at the final concentration of 18 nM were mixed with varying concentrations (0–50 μM) of rNln in artificial cerebrospinal fluid (aCSF: NaCl 126 mM, NaHCO₃ 26 mM, KCl 3 mM, KH₂PO₄ 1.4 mM, HEPES 25 mM, glucose 4 mM, MgCl₂ 1.3 mM, CaCl₂ 1.4 mM, ZnSO₄ 0.2 μM, pH 7.2) supplemented by 0.01% Triton X-100 in a 96-well plate. The volume in each well was 100 μl. Fluorescence anisotropy was measured at 25 °C on a Tecan Spark 10 M plate reader with the excitation and emission wavelengths of 485 and 535 nm, respectively. Changes in fluorescence polarization (mP) from the no Nln control were plotted against the total Nln concentration in the reaction. The data were fit to a 'one site—specific binding with ligand depletion' model in GraphPad Prism to determine the K_D values and 95% confidence intervals.

Hydrolysis of dynorphin A peptides

Hydrolysis of Dyn A (1–7), Dyn A (1–8), Dyn A (1–9), Dyn A (1–10), Dyn A (1–11), Dyn A (1–12), Dyn A (1–13), and Dyn A (1–17) (20 μM final assay concentration; obtained from Phoenix Peptides) by hNln (2 nM final assay concentration in aCSF containing 0.01% Triton X-100) was carried out in the absence in 30 μl total volume at 37 °C for 45 min. The reaction was stopped with 1 μl of 1.0 N HCl followed by freezing at – 80 °C. Quantification of each peptide was carried out by a Shimadzu Nexera Ultra High-performance LC System and a triple quadrupole Ion-Trap AB SCIEX QTRAP 5500 mass spectrometer following a protocol modified from our recent studies[13]. Chromatographic separation was achieved on a Kinetex- EVO-C18 100 Å column (1.7 μm, 50 × 2.1 mm, Phenomenex) with a mobile phase composed of solvent A (0.1% formic acid in water) and solvent B (0.1% formic acid in acetonitrile), at a flow rate of 300 μl/min with a total run time of 5 min. The gradient of solvent B was: 5% hold for 0.5 min, a linear increase from 5–45% till 2.5 min, increase to 90% in the next 0.1 min, continuation at this level from 2.6 to 3.6 min, return to 5% in the next 0.1 min, and continuation at this level until 5 min. The detection of the each Dyn peptide and its fragments were evaluated by positive polarity and multiple-reaction monitoring mode (150 ms dwell times and 5500 V). As an internal standard, each sample was spiked with DAMGO, a synthetic peptide (product 1171, Tocris Bioscience). The precursor ion of the charged state for each peptide was estimated by the mass-to-charge ratio (m/z) as M + 1, (M + 2)/2, (M + 3)/3, or (M + 4)/4 primary ions and then identified and fragmented using collision-induced dissociation voltage. The collision energies used for Dyn A (1–7) to Dyn A (1–13) were 15, 17, 25, 29, 33, 19, and 27 V, whereas for Dyn (1–17), it was 37 V. The Q1 to Q3 transitions were m/z 290.0 precursor ion to m/z 353.4 for Dyn A (1–7), m/z 327.7 precursor ion to m/z 409.9 for Dyn A (1–8), m/z 379.8 precursor ion to m/z 136.1 for Dyn A (1–9), m/z 412.3 precursor ion to m/z 136.1 for Dyn A (1–10), m/z 454.9 precursor ion to m/z 136.1 for Dyn A (1–11), m/z 369.6 precursor ion to m/z 438.4 for Dyn A (1–12), m/z 401.7 precursor ion to m/z 136.1 for Dyn A (1–13), m/z 537.5 precursor ion to m/z 136.1 for Dyn A (1–17), and m/z 514 precursor ion to m/z 134.1 for DAMGO. With Analyst software (version 1.7.2), the peak areas for each peptide and the internal standard were measured and shown as a peak area ratio (peptide peak area/internal standard peak area). The peak area ratio of the peptide to the internal standard for "no Nln" condition was arbitrarily set at 100% and compared with the peak area ratio of a sample where the peptide was incubated with Nln.

Competition of dynorphin A peptides with a fluorogenic Nln substrate

Competition of Dyn A peptides (purchased from Phoenix Peptides) with quenched fluorescence substrate Mca–Pro–Leu–Gly–Pro–D–Lys(DNP)–OH (product # M-2270, Bachem Peptides) to bind Nln was measured in a continuous enzymatic assay by documenting the increase in.

fluorescence from the cleavage of the synthetic substrate as detailed in our previous publications[13,20]. In brief, Nln was incubated with 15 µM substrate in aCSF at 37 °C (± each Dyn A peptide at 0.1–100 µM concentration, in 100 µL assay volume) and generation of the fluorescent product was continuously documented for 20 min in initial velocity conditions (SynergyMX; Biotek) where < 10% of the substrate was metabolized.

Statistical analyses

Statistical analyses and curve fitting were conducted with GraphPad Prism 7.05 software. For each enzymatic reaction, slope of the line which represents the initial velocity (V_0) for the reaction progress curve was calculated using the liner regression model of the software. For calculation of IC_{50} values, V_0 values for synthetic substrate hydrolysis by Nln in the presence of varying concentrations of each Dyn A peptide were expressed as percent within each experiment, 100% being V_0 of enzymatic reaction in the absence of a Dyn A peptide (i.e., basal activity with vehicle control). IC_{50} were calculated by fitting $\%V_0$ values into a nonlinear regression model for the three-parameter log(inhibitor) vs. response equation in Prism. Ki values were determined using the Cheng–Prusoff equation: $Ki = IC_{50}/(1 + S/K_m)$ where S is the substrate concentration (15 µM), and K_m is the K_m value for the substrate (8 µM for the quenched fluorescence substrate and hNln).

Data availability

The structure factors and atomic coordinates for the crystal structures have been deposited in the Protein Data Bank (PDB) under the following accession codes. 8VJU: dynorphin A(1–13); 8VJV: dynorphin A(1–8); 8VJW: angiotensin; 8VJY: neurotensin; 8VJX: bradykinin.

References

1. Checler, F. & Ferro, E. S. Neurolysin: From initial detection to latest advances. *Neurochem. Res.* **43**, 2017–2024 (2018).
2. Shrimpton, C. N., Smith, A. I. & Lew, R. A. Soluble metalloendopeptidases and neuroendocrine signaling. *Endocr. Rev.* **23**, 647–664 (2002).
3. Checler, F., Vincent, J. P. & Kitabgi, P. Purification and characterization of a novel neurotensin-degrading peptidase from rat brain synaptic membranes. *J. Biol. Chem.* **261**, 11274–11281 (1986).
4. Dauch, P., Vincent, J. P. & Checler, F. Molecular cloning and expression of rat brain endopeptidase 3.4.24.16. *J. Biol. Chem.* **270**, 27266–27271 (1995).
5. Checler, F. Experimental stroke: Neurolysin back on stage. *J. Neurochem.* **129**, 1–3 (2014).
6. Karamyan, V. T. The role of peptidase neurolysin in neuroprotection and neural repair after stroke. *Neural Regen. Res.* **16**, 21–25 (2021).
7. Mirali, S. *et al.* The mitochondrial peptidase, neurolysin, regulates respiratory chain supercomplex formation and is necessary for AML viability. *Sci. Transl. Med.* https://doi.org/10.1126/scitranslmed.aaz8264 (2020).
8. Teixeira, P. F. *et al.* Mechanism of peptide binding and cleavage by the human mitochondrial peptidase neurolysin. *J. Mol. Biol.* **430**, 348–362 (2018).
9. Rioli, V. *et al.* Novel natural peptide substrates for endopeptidase 24.15, neurolysin, and angiotensin-converting enzyme. *J. Biol. Chem.* **278**, 8547–8555 (2003).
10. Brown, C. K. *et al.* Structure of neurolysin reveals a deep channel that limits substrate access. *Proc. Natl. Acad. Sci. U. S. A.* **98**, 3127–3132 (2001).
11. Hines, C. S. *et al.* Allosteric inhibition of the neuropeptidase neurolysin. *J. Biol. Chem.* **289**, 35605–35619 (2014).
12. Uyar, A., Karamyan, V. T. & Dickson, A. Long-range changes in neurolysin dynamics upon inhibitor binding. *J. Chem. Theory Comput.* **14**, 444–452 (2018).
13. Jayaraman, S. *et al.* Identification and characterization of two structurally related dipeptides that enhance catalytic efficiency of neurolysin. *J. Pharmacol. Exp. Ther.* **379**, 191–202 (2021).
14. Rahman, M. S. *et al.* Discovery of first-in-class peptidomimetic neurolysin activators possessing enhanced brain penetration and stability. *J. Med. Chem.* **64**, 12705–12722 (2021).
15. Esfahani, S. H., Abbruscato, T. J., Trippier, P. C. & Karamyan, V. T. Small molecule neurolysin activators, potential multi-mechanism agents for ischemic stroke therapy. *Expert Opin. Ther. Targets* **26**, 401–404 (2022).
16. Jayaraman, S. *et al.* Peptidase neurolysin functions to preserve the brain after ischemic stroke in male mice. *J. Neurochem.* **153**, 120–137 (2020).
17. Barrett, A. J. *et al.* Thimet oligopeptidase and oligopeptidase M or neurolysin. *Methods Enzymol.* **248**, 529–556 (1995).
18. Schwarzer, C. 30 years of dynorphins—New insights on their functions in neuropsychiatric diseases. *Pharmacol. Ther.* **123**, 353–370 (2009).
19. Dahms, P. & Mentlein, R. Purification of the main somatostatin-degrading proteases from rat and pig brains, their action on other neuropeptides, and their identification as endopeptidases 24.15 and 24.16. *Eur. J. Biochem.* **208**, 145–154 (1992).
20. Wangler, N. J. *et al.* Preparation and preliminary characterization of recombinant neurolysin for in vivo studies. *J. Biotechnol.* **234**, 105–115 (2016).
21. Karamyan, V. T., Gadepalli, R., Rimoldi, J. M. & Speth, R. C. Brain AT1 angiotensin receptor subtype binding: importance of peptidase inhibition for identification of angiotensin II as its endogenous ligand. *J. Pharmacol. Exp. Ther.* **331**, 170–177 (2009).
22. Karamyan, V. T. & Speth, R. C. Enzymatic pathways of the brain renin-angiotensin system: Unsolved problems and continuing challenges. *Regul. Pept.* **143**, 15–27 (2007).
23. Machado, M. F. *et al.* The role of Tyr605 and Ala607 of thimet oligopeptidase and Tyr606 and Gly608 of neurolysin in substrate hydrolysis and inhibitor binding. *Biochem. J.* **404**, 279–288 (2007).
24. Oliveira, V. *et al.* Selective neurotensin-derived internally quenched fluorogenic substrates for neurolysin (EC 3.4.24.16): Comparison with thimet oligopeptidase (EC 3.4.24.15) and neprilysin (EC 3.4.24.11). *Anal. Biochem.* **292**, 257–265 (2001).
25. Oliveira, V. *et al.* Substrate specificity characterization of recombinant metallo oligo-peptidases thimet oligopeptidase and neurolysin. *Biochemistry* **40**, 4417–4425 (2001).
26. Bar-Even, A. *et al.* The moderately efficient enzyme: Evolutionary and physicochemical trends shaping enzyme parameters. *Biochemistry* **50**, 4402–4410 (2011).
27. Lim, E. J. *et al.* Swapping the substrate specificities of the neuropeptidases neurolysin and thimet oligopeptidase. *J. Biol. Chem.* **282**, 9722–9732 (2007).

28. Ray, K., Hines, C. S. & Rodgers, D. W. Mapping sequence differences between thimet oligopeptidase and neurolysin implicates key residues in substrate recognition. *Protein Sci.* **11**, 2237–2246 (2002).
29. Emsley, P., Lohkamp, B., Scott, W. G. & Cowtan, K. Features and development of Coot. *Acta Crystallogr. D Biol. Crystallogr.* **66**, 486–501 (2010).
30. Adams, P. D. *et al.* PHENIX: A comprehensive Python-based system for macromolecular structure solution. *Acta Crystallogr. D Biol. Crystallogr.* **66**, 213–221 (2010).

Acknowledgements

Author contributions

Ke Shi: conceptualization, validation, investigation, visualization. Sounak Bagchi: investigation, visualization. Jordis Bickel: investigation, visualization. Shiva H. Esfahani: investigation, visualization. Lulu Yin: investigation, visualization. Tiffany Cheng: investigation, visualization. Vardan T. Karamyan: conceptualization, investigation, visualization, writing—original draft, writing—review & editing, supervision, funding acquisition. Hideki Aihara: conceptualization, investigation, visualization, writing—original draft, writing—review & editing, supervision, funding acquisition. All authors contributed to the generation of presented data and figures. V.T.K. and H.A. wrote the main manuscript text. All authors reviewed the manuscript.

Funding

Competing interests

The authors declare no competing interests.

Additional information

Supplementary Information The online version contains supplementary material available at https://doi.org/10.1038/s41598-024-67639-w.

Correspondence and requests for materials should be addressed to V.T.K. or H.A.

Reprints and permissions information is available at www.nature.com/reprints.

Publisher's note Springer Nature remains neutral with regard to jurisdictional claims in published maps and institutional affiliations.